Journal of Materials Chemistry C

ROYAL SOCIETY OF CHEMISTRY

PAPER

View Article Online
View Journal | View Issue

Cite this: J. Mater. Chem. C, 2024, 12, 5175

Ionic liquid-regulated PbI_2 layers and defect passivation for efficient perovskite solar cells†

Yonggui Sun,‡[ab] Ruiyuan Hu,‡*[a] Fei Wang,[bc] Taomiao Wang,[ab] Xiao Liang,[bc] Xianfang Zhou,[bc] Guo Yang,[b] Yongjun Li,[ab] Fan Zhang,[ab] Quanyao Zhu,[c] Xing'ao Li*[a] and Hanlin Hu *[b]

In recent years, substantial progress has been made in improving the power conversion efficiency of perovskite solar cells (PSCs). However, persistent defects continue to impede their further advancement. Although ionic liquids (ILs) have been extensively utilized for perovskite defect passivation, their application, particularly in two-step methods, remains limited. In this study, we introduced formamidine acetate (FAAc) as a liquid additive, incorporated into the PbI_2 precursor solution to finely regulate perovskite crystal growth. Utilizing a two-step method, we meticulously investigated the interaction of FAAc with perovskite components, laying the groundwork for effective defect passivation. Our systematic exploration delved into the nuanced influence of ILs on perovskite solar cells, including thin film morphology, optical properties, defect density, and overall device performance. Importantly, ILs facilitated the conversion of PbI_2 into a perovskite material while reducing residual PbI_2 during the perovskite crystallization process, thereby significantly improving the performance of PSCs, including device stability. Though defect passivation during perovskite formation facilitated the conversion of PbI_2 and the modulation of thin film morphology, the photoelectric conversion efficiency of the treated PSCs approached an impressive 24.41%. Even after undergoing 2000 hours of aging in dry air, the efficiency remained at above 96% of the initial level. This research marks a pivotal step forward in the realm of PSCs. Our findings not only showcase the potential of ionic liquids in the two-step preparation of PSCs but also highlight their pivotal role in enhancing the efficiency and stability.

Received 5th February 2024,
Accepted 7th March 2024

DOI: 10.1039/d4tc00500g

rsc.li/materials-c

Introduction

Over the past decade, perovskite solar cells (PSCs) have garnered significant attention owing to their remarkable photovoltaic performance. Notably, the power conversion efficiency (PCE) of single-cell PSCs has surged from a mere 3.8% to an impressive 26.1%, placing them on par with commercially available silicon solar cells.[1–4] Consequently, PSCs have emerged as a particularly promising technology due to their exceptional light absorption capabilities, tunable band gaps, straightforward fabrication processes, and high PCE, which makes them the subject of extensive research.[5–8] Generally, the absorber is the crucial part of PSCs, and is generally fabricated by a one-step antisolvent method and a two-step sequential deposition method.[9–11] After comparison, the latter without the toxic antisolvent is found to be superior due to the control over crystal quality, improved film morphology and scalable operation, especially for commercialization.[12,13] In the two-step method, perovskite thin films are obtained by infiltrating the organic ammonium salt in PbI_2 thin films. Unfortunately, undesired crystal orientations, non-radiative recombination and excess PbI_2 would be generated during the formation of perovskite thin films, which restrict the PCE and stability of PSCs.[14–19] Therefore, the fabrication of PbI_2 thin films lays an important foundation to obtain excellent perovskite thin films after reacting with organic ammonium salts in the two-step method.

To modulate PbI_2 thin films, a range of approaches have been adopted, including solvent engineering and additive engineering. In particular, additive engineering is an effective way to modify the PbI_2 porosity and perovskite

[a] Jiangsu Provincial Engineering Research Center of Low Dimensional Physics and New Energy & School of Science, Key Laboratory for Organic Electronics and Information Displays & Institute of Advanced Materials (IAM), Jiangsu National Synergistic Innovation Center for Advanced Materials (SICAM), Nanjing University of Posts and Telecommunications, Nanjing 210023, China.
E-mail: ruiyuanhu@njupt.edu.cn, lixa@njupt.edu.cn, hanlinhu@szpu.edu.cn
[b] Hoffmann Institute of Advanced Materials, Shenzhen Polytechnic, 7098 Liuxian Boulevard, Shenzhen 518055, China
[c] State Key Laboratory of Advanced Technology for Materials Synthesis and Processing, School of Materials Science and Engineering, Wuhan University of Technology, Wuhan 430070, China

† Electronic supplementary information (ESI) available. See DOI: https://doi.org/10.1039/d4tc00500g

‡ Y. S. and R. H. contributed equally to this work.

crystallization.[20,21] It was reported that hexamethylphosphoramide (HMPA) with high binding affinity and high boiling point was incorporated into the PbI_2 precursor to modify the morpgology and internal structure of the PbI_2 layer, which helped the infiltration of the second-step organic salt to form the perovskite thin film with uniform surface, large grains and reduced defects.[22] Chen and coworkers found that the modified PbI_2 thin film with 4-(aminomethyl) benzonitrile hydrochloride (AMBNCl) facilitated the fabrication of compact perovskite films with large grains and pinhole-free structures,[23] which leads to the passivation of defects of Pb^{2+}, modulation of the energy level array and alleviation of nonradiative recombination. Fang's group introduced pentafluoroanilinium trifluoromethanesulfonate (PFAT) into PbI_2 precursor solutions to modulate the nucleation and crystallization of the PbI_2 films.[24] PFAT facilitated the secondary growth of PbI_2 clusters and early formation of perovskite phases. With the reduced Gibbs free energy of the porous PbI_2, the perovskite was crystallized with preferential orientation, enlarged grains, reduced defects and decreased PbI_2 residues, resulting in an impressive PCE of 24.52% with an enhanced fill factor (FF) of 82.8%.

Among the multitude of additives to regulate the growth of perovskite films, ionic liquids (ILs) have gained widespread recognition. ILs are particularly appealing due to their nonvolatile nature, making them an environmentally friendly choice. Moreover, ionic liquids possess other commendable characteristics, such as a simple chemical structure, high carrier mobility, and excellent thermal and chemical stability.[25–27] Consequently, ILs as additives in perovskite film formation have attracted much attention. In particular, formamidine acetate (FAAc) is extensively employed as the additive in PSCs, owing to its low molecular weight and low melting point. Dong's group modified perovskite films by introducing FAAc and obtained uniform perovskite films with enhanced crystalline quality, film morphology and low trap states.[28] Moreover, FAAc is also an effective interfacial additive between the electron transport layer (ETL) and perovskite layer, such as TiO_2/perovskite and SnO_2/perovskite.[29,30] The connection of the FA^+ between the ETL and perovskite promotes electron transport, and the amino group ($-NH_2$) and carboxyl group (–COOH) of FAAc passivates the defect at the ETL/perovskite interface, resulting in the improved device performance. However, it is important to note that there has been limited research regarding the use of ILs in the regulation of perovskite crystals using the two-step method. As a result, there is a pressing need for further exploration and a deeper understanding of how ILs can be effectively employed in the two-step process. Such research may hold the key to unlocking even greater advancements in perovskite solar cell technology, with the potential to significantly impact the field of renewable energy and environmental sustainability.

In this study, FAAc was employed as an additive to regulate the growth of PbI_2 thin films for the subsequent crystallization of perovskites. Our investigation focuses on several key parameters, including IL's action mechanism, film morphology, perovskite film photovoltaic properties and device performance. Nuclear magnetic resonance spectroscopy (NMR), X-ray photoelectron spectroscopy (XPS) and Fourier transform infrared spectroscopy (FTIR) were used to analyze the chemical interaction characteristics between C═O and Pb^{2+}, as well as N–H bonds in FAAc and the I^- anions, which provided a basis for the defects formed during the crystallization process of the perovskite. X-ray diffraction (XRD) analysis confirmed that the introduction of ILs promotes the transformation of PbI_2 and organic cations into a perovskite, consequently reducing the residue of PbI_2 in the final product. This reduction significantly enhanced the stability of the PSCs. Furthermore, the addition of ILs greatly improved the morphology of perovskite films, and from the scanning electron microscopy (SEM) and atomic force microscopy (AFM) results, the modified films were found to have a larger grain size and lower surface roughness. The enhanced film quality and the passivation of defects by ILs contribute to the suppression of nonradiative carrier recombination. As a result, the extended carrier lifetime led to improved device performance. Finally, the PSCs modified with ILs achieved a champion PCE of 24.41%, surpassing that of control devices by 22.12%. This study provides an in-depth exploration of the crystallization mechanism of IL-modified perovskites, showcasing the potential of ILs in the two-step preparation of photovoltaic devices. It advances our understanding of how ILs can be applied to enhance the performance of PSCs.

Results and discussion

In accordance with previous literature, perovskite films were fabricated by a traditional two-step method, as illustrated in Fig. S1 (ESI†).[31] The Cs-doped PbI_2 solution was spin-coated on the SnO_2/ITO substrate to form a PbI_2 film after drying for 1 min. The organic salt solution (FAI, MAI and MABr) was then spin-coated on the surface of the PbI_2 film, forming the control perovskite film after thermal annealing. For the IL-modified perovskite film, FAAc was introduced into the PbI_2 precursor solution, the structural formula of which is presented in Fig. S2 (ESI†). The schematic representation of the perovskite layer treated with FAAc reveals that the primary modification mechanism involves the coordination of the carbonyl group (C═O) in FAAc with the uncoordinated Pb^{2+} ions. This coordination effectively passivates Pb defects within the perovskite structure. Furthermore, a strong hydrogen bond forms between the N–H bond in FAAc and the iodine (I) ions, leading to a reduction in I defects, as depicted in Fig. 1a.

This result was subsequently confirmed by a series of chemical analyses. The initial characterization was performed using XPS, and the full spectrum of XPS is shown in Fig. S3 (ESI†). In the XPS spectra of Pb (Fig. 1b), the control perovskite film exhibits two distinct peaks at 143.4 eV and 138.5 eV, corresponding to Pb $4f_{5/2}$ and Pb $4f_{7/2}$ signals, respectively. In contrast, the perovskite films modified with FAAc display a noticeable shift in Pb 4f peaks towards lower binding energy. Specifically, the $4f_{5/2}$ peak shifts to 143.2 eV, and the $4f_{7/2}$ peak

shifts to 138.3 eV. This shift is primarily attributed to the interaction of C=O in FAAc, which contributes electrons to form chelating bonds with Pb^{2+} ions. It is worth noting that the control perovskite film shows obvious Pb0 peaks at 141.4 eV and 136.4 eV, and the Pb0 peak of the IL-modified film disappears, indicating a reduction in the residue of unreacted PbI_2 after the addition of ILs. This outcome underscores the effectiveness of ILs in enhancing the purity and stability of the perovskite structure. The XPS spectra of I are depicted in Fig. 1c. In the control perovskite film, two discernible peaks are evident at 630.8 eV and 619.3 eV corresponding to the binding energy of I $3d_{3/2}$ and I $3d_{5/2}$, respectively. Notably, the positions of these two I 3d peaks shift towards lower binding energies following the modification with FAAc, indicating a strong chemical interaction between FAAc and I^- within the perovskite structure. The XPS data provided compelling evidence of the strong chemical interaction between FAAc and the constituent elements of the perovskite. This interaction was pivotal in passivating defects within the perovskite material and impeding the migration of ions. To gain deeper insights into the interaction between ILs and perovskites, FTIR was performed on both FAAc and FAAc/PbI_2 solutions. The results showed that the characteristic peak associated with the C=O bond in FAAc initially appeared at the wavenumber of 1712 cm^{-1}. Upon the introduction of PbI_2, the vibration frequency of C=O was proven to be increased on account of the shift in C=O vibration to 1719 cm^{-1}, suggesting that the C=O group donates an electron pair to coordinate with the under-coordinated Pb atoms, forming a robust C=O–Pb chelate bond (as demonstrated in Fig. 1d).

To further validate these findings, NMR spectroscopy was employed to investigate the bonding interactions between FAAc and the perovskite. In the ^{13}C NMR spectra, a noticeable shift is observed in the C=O peak, moving from 176.8 ppm in FAAc to 177.4 ppm in FAAc-PbI_2. This shift provides additional evidence of the interaction between the COO– group in FAAc and residual Pb^{2+} ions (as illustrated in Fig. 1e). In addition, ^1H NMR spectra were obtained to explore the interaction between FAAc and I^- ions. For the FAAc and FAAc-PbI_2 solution, the amino hydrogen spectrum in FAAc shifted from 7.72 to 7.78 ppm owing to the strong N–H···I hydrogen bond between the FAAc and I^- (Fig. 1f). In summary, the

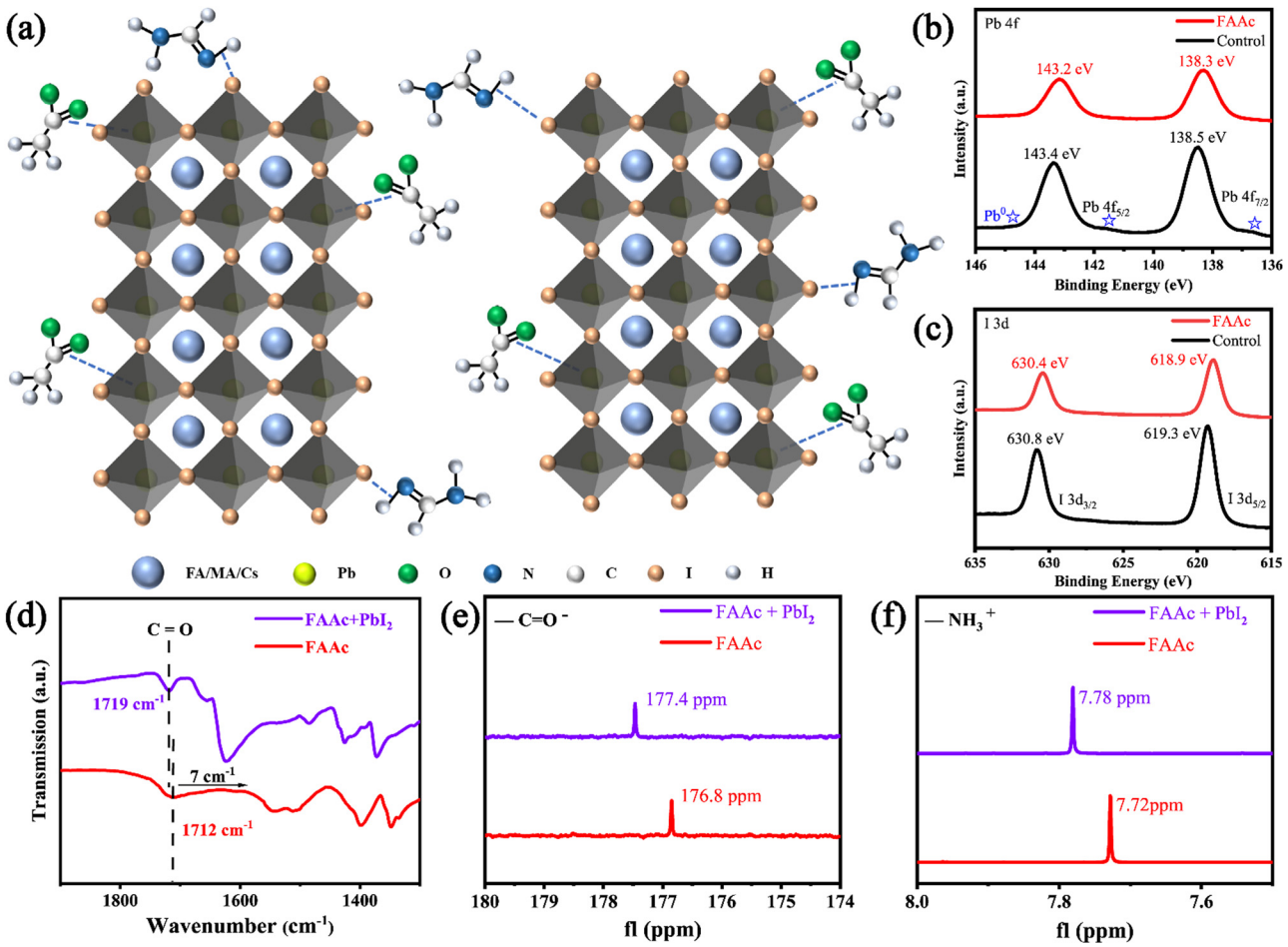

Fig. 1 (a) Schematic diagram of FAAc passivation Pb defects and I defects. The high-resolution XPS spectrum of (b) Pb 4f scan and (c) I 3d scan from control and FAAc-modified perovskite films. (d) FTIR spectrum of FAAc and FAAc-PbI_2 solutions in magnified forms. (e) ^{13}C and (f) ^1H NMR spectra of FAAc and FAAc-PbI_2 solutions.

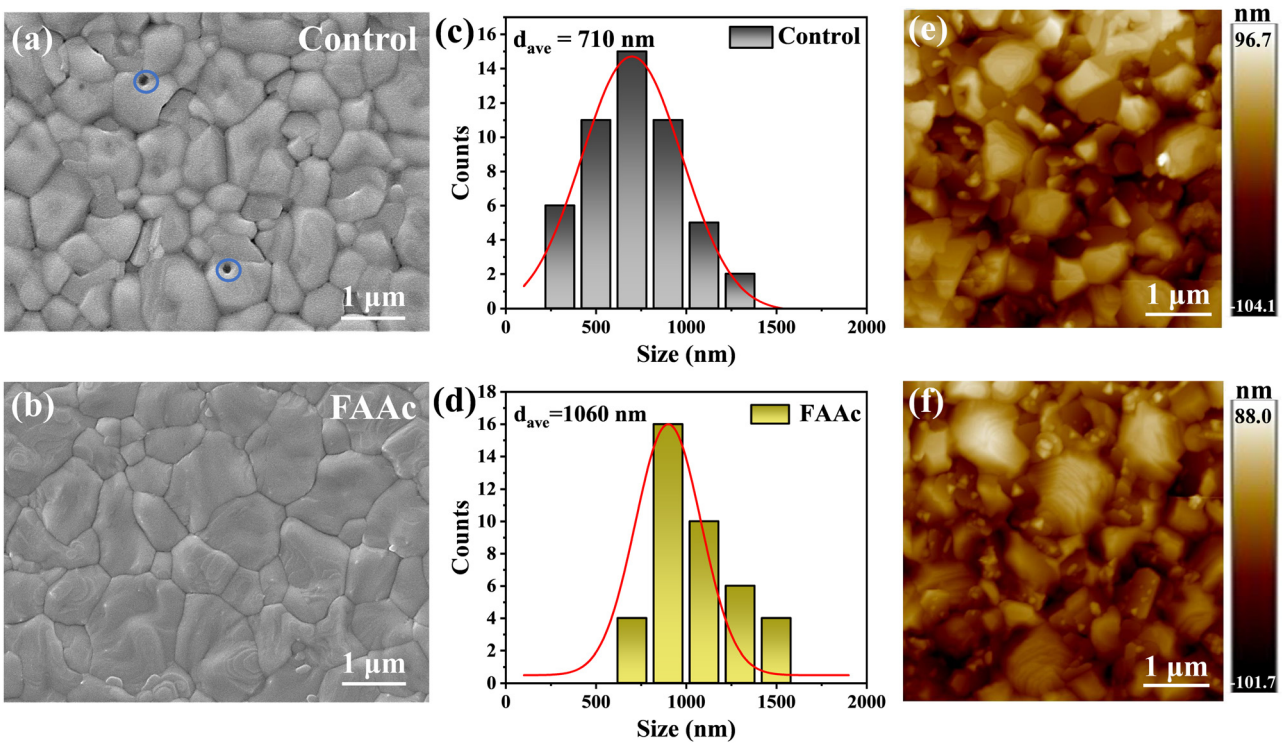

Fig. 2 Top-view SEM images of (a) control and (b) FAAc modified-perovskite films. The grain size distribution of (c) control and (d) FAAc modified-perovskite films. AFM images of (e) control and (f) FAAc modified-perovskite films.

combination of XPS, FTIR, and NMR analyses provides a comprehensive understanding of the intricate chemical interactions occurring between FAAc and the perovskite material. These interactions play a pivotal role in defect passivation and ion migration inhibition within the perovskite structure, making these findings highly significant in the context of perovskite-based materials and their potential applications.

As shown in Fig. 2a and b, our investigation into the transformation of FAAc modified perovskite films involved acquiring top-view images of both the control and FAAc modified perovskite films using SEM analysis. Compared with the original perovskite film (Fig. 2a), the FAAc modified film exhibited higher quality of perovskite grains, marked by a decrease in PbI_2 and an increase in grain size (Fig. 2b). It is worth noting that the presence of pinholes can be clearly observed in the unmodified perovskite film, which is detrimental to the charge transport. In contrast, the FAAc-modified film displayed a conspicuous absence of pinholes, resulting in a denser structure. The enhancement in film quality primarily stems from the regulation of grain nucleation and growth mechanisms.[24] The hydrophobic properties are also a criterion of the perovskite film quality. The contact angle test was conducted, as depicted in Fig. S4 (ESI†). The modified film exhibited a notably higher contact angle, indicating that the FAAc modification enhanced the film's hydrophobic properties, which improved the stability. To understand the mechanism by which ILs improve perovskite films, we performed SEM testing to examine the top view of PbI_2 films before and after treatment with ILs, as illustrated in Fig. S5 (ESI†). The FAAc-modified film showed larger pores, which is conducive to better penetration of organic salts into the PbI_2 film to promote the formation of the perovskite structure. Furthermore, FAAc was uniformly distributed in the PbI_2 film, as indicated by the presence of N and O elements on the energy dispersive spectrometry (EDS) spectrum (Fig. S6, ESI†). Statistical analysis of the grain size demonstrated a substantial increase, with the average grain size increasing from 710 nm (Fig. 2c) to 1080 nm (Fig. 2d). The grain size enhancement is a direct result of the interaction between ILs and the perovskite. The introduction of FAAc can lead to a chemical interaction with PbI_2, thus delaying the crystal nucleation process of the perovskite, which in turn increases the grain size of the perovskite. This interaction plays a pivotal role in regulating the uniform growth of the perovskite, effectively restraining non-radiative carrier recombination at grain boundaries, and thereby enhancing its transport performance. As shown in Fig. 2e and f, AFM further verified that FAAc can effectively regulate the increase of perovskite grains, which is consistent with the SEM results.

To gain a more profound insight into the impact of FAAc on perovskite films, we obtained XRD patterns of both controlled and FAAc-modified perovskite films. As shown in Fig. 3a, the diffraction peak at 14.02° corresponds to the (110) crystal plane in the perovskite and the position of the diffraction peak remained largely unaltered before and after modification, which indicated that ILs have negligible effect on the lattice change of perovskite after modification. At the same time, it is crucial to emphasize that in comparison to the control perovskite film, the diffraction peak intensity corresponding to PbI_2 at

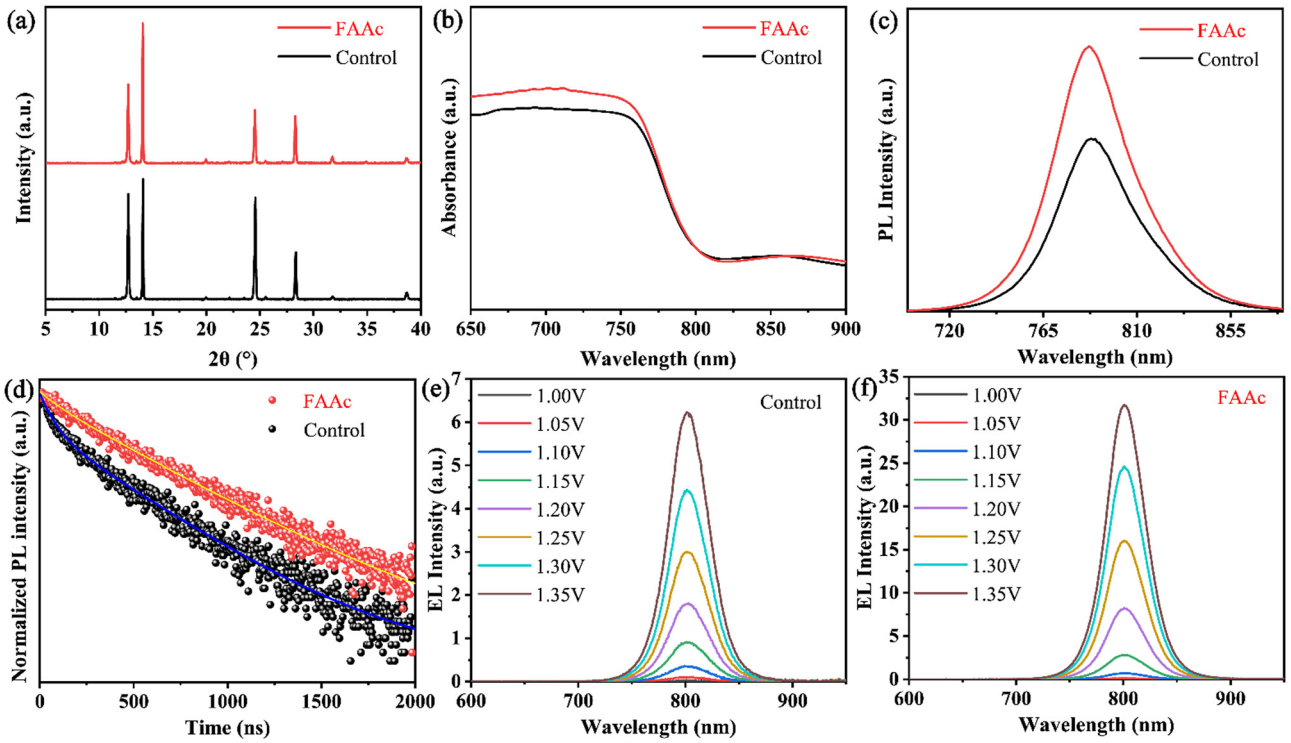

Fig. 3 (a) X-ray diffraction spectra of control and FAAc-modified perovskite films. (b) UV-visible absorption spectra of the control and FAAc-modified perovskite films. (c) PL and (d) time-resolved PL spectra of the glass/control and FAAc-modified perovskite samples. EQE-EL measurements of (e) control and (f) FAAc-modified PSCs under different bias voltages.

12.70° significantly diminishes after FAAc modification. This reduction indicates the effective mitigation of PbI_2 residues in the presence of ILs, corroborating the findings from the SEM analysis. This reduction in PbI_2 residues is of paramount importance for enhancing the stability of the device.[32,33] Subsequently, in the ultraviolet-visible (UV-vis) and photoluminescence (PL) test results, the control and FAAc-modified perovskite films exhibit nearly identical absorption thresholds and photoluminescence positions, further revealing no discernible effect on the lattice structure, aligning with the XRD results. Importantly, the UV-vis absorption spectrum highlights an enhanced light absorption capacity of the FAAc-modified film, which enhanced light capture and reduced carrier non-radiative recombination (shown in Fig. 3b). In addition, the PL and TRPL test results showed that FAAc-modified films exhibited enhanced PL emission and longer carrier lifetimes compared to control films, meaning that carrier non-radiative recombination is reduced, which is consistent with UV-vis test results (Fig. 3c and d). The above results underscored the positive impact of FAAc-induced defect passivation, optimizing the quality of the perovskite film while effectively inhibiting carrier non-radiative recombination. Subsequently, we further investigated the effect of FAAc on reducing the non-radiative recombination center under identical bias voltage. The electroluminescence intensity of the FAAc-modified device was significantly enhanced compared with the control device (Fig. 3e and f), indicating the effective inhibition of non-radiative recombination consistent with the results of PL.

To evaluate the trap state density (n_{trap}) in the device, we prepared a pure electronic device (ITO/SnO_2/perovskite/PCBM/Au) to test the space charge limiting current (SCLC) curve. The dark J–V curve can be divided into three areas, namely Ohmic, TFL (trap-filled limit) and child regions. n_{trap} is calculated using the threshold voltage (V_{TFL}) at the point of the Ohmic and TFL regions following the equation:

$$n_{trap} = \frac{2\varepsilon\varepsilon_0 V_{TFL}}{eL^2} \quad (1)$$

where ε_0 is the vacuum permittivity, ε is the relative permittivity, e is the elementary charge, and L is the thickness of the perovskite film.[34] The V_{TFL} of the control device was 0.479 V (Fig. 4a), while the V_{TFL} of the FAAc-modified device was significantly reduced to 0.131 V (Fig. 4b). The n_{trap} value before and after modification can be calculated as 3.57×10^{15} cm^{-2} and 9.76×10^{14} cm^{-2} (shown in Fig. 4c). The above test results further verified the previous conclusion that the introduction of FAAc into perovskites can effectively inhibit the formation of defects, which in turn can inhibit the carrier non-radiative recombination and enhance the charge transport performance.

The Mott–Schottky curve obtained using capacitance and voltage values played a crucial role in our comprehensive analysis of the carrier combination and transport in the device. The results revealed that the device internal potential (V_{bi})

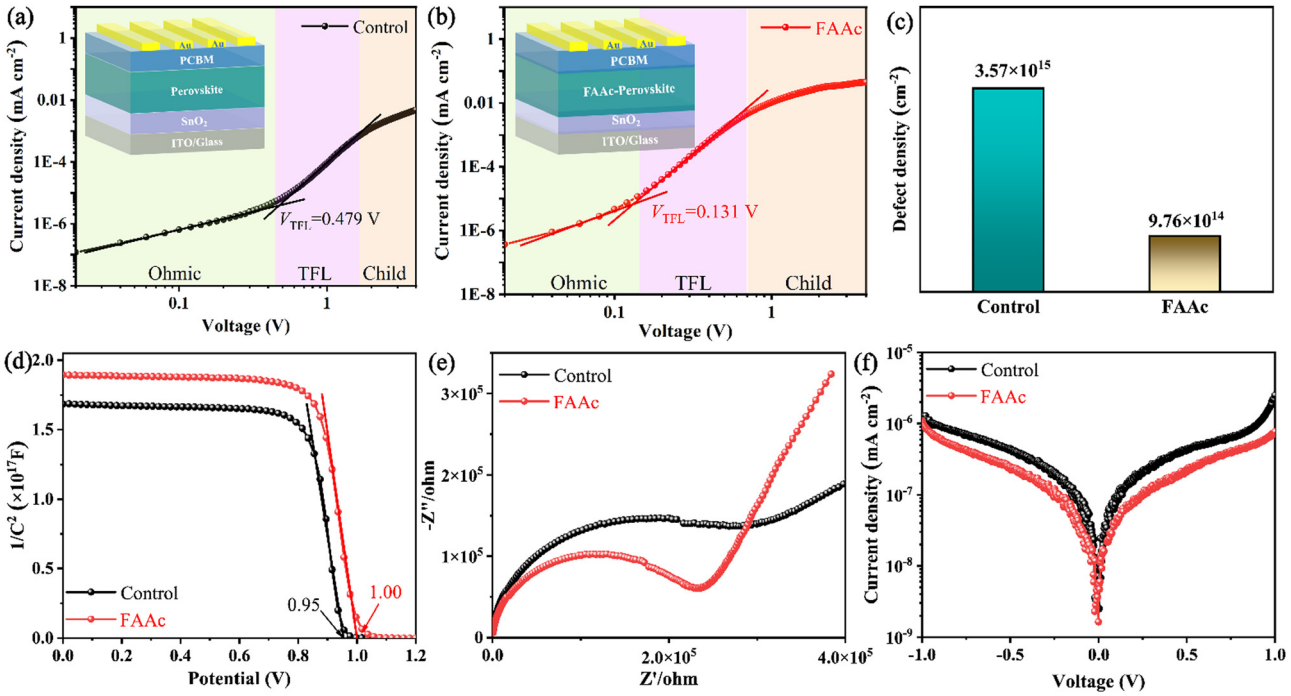

Fig. 4 (a) and (b) Dark J–V curves of the devices with the structure of ITO/SnO_2/control or FAAc-modified perovskite/PCBM/Au. (c) Statistics for defect density computed from the dark J–V curves. (d) Mott–Schottky plots of control and FAAc-treated devices. (e) Nyquist plots and (f) J–V curves under dark conditions of control and FAAc-treated devices.

increases from 0.95 V to 1.00 V after FAAc modification (Fig. 4d), which caused an increase in the open-circuit voltage (V_{oc}) due to the enhanced carrier extraction and transmission rate.[35] Simultaneously, the electrochemical impedance spectroscopy (EIS) test was carried out at a bias voltage of 0 V to discuss the charge transport performance (Fig. 4e). The arcs in the high- and low-frequency regions represent the charge transfer resistance (R_{ct}) and the composite resistance (R_{rec}), respectively. The test results indicated that the FAAc-modified device exhibited a reduced R_{ct} and an elevated R_{rec} compared to the control device, which signified enhanced charge transportation and effectively mitigated charge recombination. In addition, the decrease in the dark current density for the FAAc-modified device further indicated that the charge transfer was enhanced, concurrently leading to a reduction in the leakage current (Fig. 4f).

In order to delve deeper into the influence of FAAc on the device performance, we prepared control and FAAc-modified PSCs with a planar structure of ITO/SnO_2/perovskite/Spiro-OMeTAD/Au, as visually represented in Fig. 5a. From the cross-sectional SEM images of both complete devices, it can be observed that the grains of the FAAc-modified perovskite layer can grow better in the vertical direction and they are significantly larger and the number of grain boundaries is significantly reduced, in accordance with the previous top-view SEM results (Fig. 5b and c). To determine the optimal FAAc concentration for enhancing the device performance, we performed experiments on modified devices with different concentrations, and the device photovoltaic parameters were obtained and are shown in Table S1 (ESI†). With the optimal FAAc concentration, the photovoltaic parameters of the device have significantly improved. Compared with the PCE of 22.12% for the control device, the FAAc modified device reached a champion PCE of 24.41%, for which the V_{oc} is 1.193 V, J_{sc} is 25.28 mA cm^{-2}, and FF is 80.92% (Fig. 5d). To verify the repeatability of ILs to improve device efficiency, we prepared 40 control devices as well as FAAc-modified devices and measured their photovoltaic performance, as shown in Fig. S7 (ESI†). Through the statistics of V_{oc}, J_{sc}, FF and PCE, it can be seen that the improvement of PCE is mainly due to the improvement of V_{oc} and FF, while J_{sc} has not changed much. Through the bar chart of PCE, we can more intuitively see that the efficiency of FAAc modified devices is significantly improved and has good reproducibility (Fig. S8, ESI†). And we tested the external quantum efficiency (EQE) of the solar spectrum, and the results were consistent with the J_{sc} values obtained in the J–V curve of FAAc-modified PSCs (Fig. 5e). The steady-state PCE of PSCs before and after FAAc processing was evaluated using maximum power point tracking, and the results showed that the devices exhibited up to 21.45% and 24.28% steady-state PCE before and after processing, respectively (Fig. 5f).

While the PCE remains a pivotal metric for characterizing PSCs, it is crucial to address the equally important aspect of their long-term operational stability.[36] First, we placed control and FAAc-modified perovskite films in a 50% relative humidity (RH) environment for 50 days at room temperature. Through XRD analysis performed both before and after storage, a

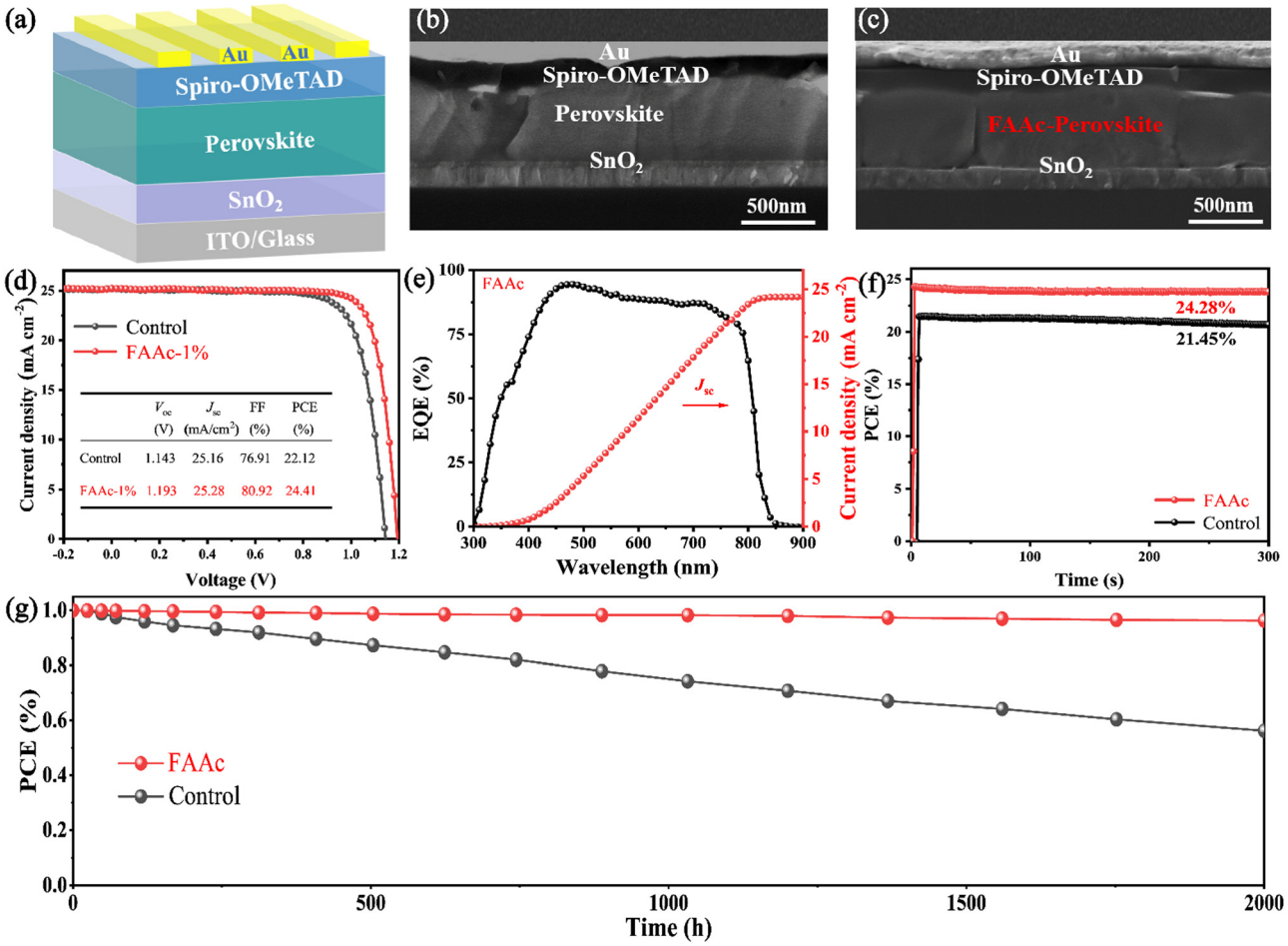

Fig. 5 (a) The schematic diagram of the device structure. Cross-sectional SEM image of the (b) control and (c) FAAc-modified perovskite device structures. (d) *J*–*V* curves of the control and FAAc-modified PSCs. (e) EQE and the integrated J_{sc} of FAAc-PSCs. (f) Steady-state PCE at the maximum power point for the control and FAAc-modified PSCs. (g) Stability test of devices.

significant increase in the signal intensity of PbI_2 at 12.7° degrees was observed in the control film after 50-day storage. However, for FAAc-modified films, the PbI_2 signal enhancement was not obvious at 12.7°, indicating a substantial improvement in film stability (as represented in Fig. S9, ESI†). Under the same conditions, we measured UV-vis absorption by leaving the film for 50 days, and the results showed that the absorption attenuation of the FAAc-modified perovskite film was much lower than that of the control film (Fig. S10, ESI†). Therefore, the introduction of FAAc into the PbI_2 layer to achieve crystallization regulation of the perovskite can reduce the residual PbI_2 in the perovskite layer, and thus enhance the overall stability of the perovskite film. The increase in the stability of FAAc-modified perovskite films indicates that the hydrophobic capacity of the film is enhanced, which echoes the increase of the contact angle of the film after the modification mentioned above. Fig. 5g shows the PCE values of an unpackaged control device and an FAAc modified device over time. The results show that the durability of the device after the unpackaged FAAc treatment is greatly improved, maintaining 96% of its initial PCE even after 2000 h in a dry environment. This remarkable enhancement in durability bodes well for the practical and long-term application of FAAc-modified PSCs.

Conclusions

In summary, the introduction of FAAc effectively passivates the defects generated during the perovskite crystal crystallization process. This strategic addition resulted in significant improvements in perovskite thin film morphology, manifesting as larger grain sizes and the elimination of pinholes. This transformation was confirmed through NMR, XPS analysis, and FTIR, collectively affirming the substantial interaction between FAAc and perovskite materials. By passivating defects with ILs and refining the surface characteristics of perovskite films, the non-radiative recombination of charge carriers was notably suppressed, and the charge transport properties were enhanced, thereby improving the overall performance of photovoltaic devices. Moreover, the stability of the FAAc-modified device showed remarkable improvement. Notably, FAAc-modified PSCs achieved a champion PCE of 24.41%, surpassing the efficiency of the control device of 22.12%. This achievement

highlights the significance of our research, advancing our understanding of defect passivation mechanisms employed using ILs and providing valuable insights into the practical application of ILs in the two-step preparation of perovskite photovoltaic devices.

Conflicts of interest

There are no conflicts to declare.

Acknowledgements

We acknowledge the financial support from the Natural Science Research Start-up Foundation of Recruiting Talents of Nanjing University of Posts and Telecommunications (Grant No. NY222027), the Natural Science Foundation of Jiangsu Higher Education Institutions of China (Grant No. TJ222038), the Guangdong Basic and Applied Basic Research Foundation (No. 2023A1515011677), and the Shenzhen Science and Technology Innovation Commission (Project No. 20220811205532001).

Notes and references

1 G. W. K. Moore, S. E. L. Howell, M. Brady, X. Xu and K. McNeil, *Nat. Commun.*, 2021, **12**, 1.
2 G. Wu, R. Liang, M. Ge, G. Sun, Y. Zhang and G. Xing, *Adv. Mater.*, 2022, **34**, 2105635.
3 H. Min, D. Y. Lee, J. Kim, G. Kim, K. S. Lee, J. Kim, M. J. Paik, Y. K. Kim, K. S. Kim, M. G. Kim, T. J. Shin and S. Il Seok, *Nature*, 2021, **598**, 444–450.
4 F. Wang, C. ye Ge, D. Duan, H. Lin, L. Li, P. Naumov and H. Hu, *Small Struct.*, 2022, **3**, 2200048.
5 Z. Chen, Q. Cheng, H. Chen, Y. Wu, J. Ding, X. Wu, H. Yang, H. Liu, W. Chen, X. Tang, X. Lu, Y. Li and Y. Li, *Adv. Mater.*, 2023, **35**, 2300513.
6 Z. Wei, Y. Zhao, J. Jiang, W. Yan, Y. Feng and J. Ma, *Chin. Chem. Lett.*, 2020, **31**, 3055–3064.
7 J. Song, H. Liu, W. Pu, Y. Lu, Z. Si, Z. Zhang, Y. Ge, N. Li, H. Zhou, W. Xiao, L. Wang and M. Sui, *Energy Environ. Sci.*, 2022, **15**, 4836–4849.
8 H. Hu, M. Qin, P. W. K. Fong, Z. Ren, X. Wan, M. Singh, C. J. Su, U. S. Jeng, L. Li, J. Zhu, M. Yuan, X. Lu, C. W. Chu and G. Li, *Adv. Mater.*, 2021, **33**, 2006238.
9 C. Xu, Z. Liu and E. C. Lee, *J. Mater. Chem. C*, 2020, **8**, 15860–15867.
10 T. Sen Su, T. E. Fan, H. K. Si, D. A. Le, N. Perumbalathodi and T. C. Wei, *Sol. RRL*, 2021, **5**, 2100109.
11 H. Chen, *Adv. Funct. Mater.*, 2017, **27**, 1605654.
12 Y. Du, Y. Wang, J. Wu, Q. Chen, C. Deng, R. Ji, L. Sun, L. Tan, X. Chen, Y. Xie, Y. Huang, Y. Vaynzof, P. Gao, W. Sun and Z. Lan, *InfoMat*, 2023, **5**, e12431.
13 C. H. Chen, Y. H. Lou, K. L. Wang, Z. H. Su, C. Dong, J. Chen, Y. R. Shi, X. Y. Gao and Z. K. Wang, *Adv. Energy Mater.*, 2021, **11**, 2101538.
14 J. Holovský, A. Peter Amalathas, L. Landová, B. Dzurňák, B. Conrad, M. Ledinský, Z. Hájková, O. Pop-Georgievski, J. Svoboda, T. C. J. Yang and Q. Jeangros, *ACS Energy Lett.*, 2019, **4**, 3011–3017.
15 Z. Yang, X. Cao, G. Niu, Y. Wang, Y. Dong, S. Cao, W. Liu, X. Wang, Y. Liu and J. Wang, *Chem. Eng. J.*, 2023, **464**, 142720.
16 E. L. Lim and Z. Wei, *J. Energy Chem.*, 2024, **90**, 504–510.
17 L. Zhang, K. Cao, J. Qian, Y. Huang, X. Wang, M. Ge, W. Shen, F. Huang, M. Wang, W. Zhang, S. Chen and T. Qin, *J. Mater. Chem. C*, 2020, **8**, 17482–17490.
18 J. Tao, Z. Yu, X. Liu, J. Xue, J. Shen, H. Guo, W. Kong, G. Fu and S. Yang, *J. Mater. Chem. C*, 2022, **10**, 8414–8421.
19 H. Zhang, F. T. Eickemeyer, Z. Zhou, M. Mladenović, F. Jahanbakhshi, L. Merten, A. Hinderhofer, M. A. Hope, O. Ouellette, A. Mishra, P. Ahlawat, D. Ren, T. Sen Su, A. Krishna, Z. Wang, Z. Dong, J. Guo, S. M. Zakeeruddin, F. Schreiber, A. Hagfeldt, L. Emsley, U. Rothlisberger, J. V. Milić and M. Grätzel, *Nat. Commun.*, 2021, **12**, 3383.
20 X. Liang, D. Duan, M. B. Al-Handawi, F. Wang, X. Zhou, C. Yye Ge, H. Lin, Q. Zhu, L. Li, P. Naumov and H. Hu, *Sol. RRL*, 2023, **7**, 2200856.
21 Y. Li, X. Sun, Y. Li, F. Deng, S. Li and X. Tao, *Sol. RRL*, 2023, **7**, 2201132.
22 J. Talbot, P. Hahn, L. Kroehling, H. Nguyen, D. Li and D. R. Littman, *Nature*, 2020, **579**, 575–580.
23 X. Chen, J. Wu, G. Li, Y. Du, Q. Chen, C. Deng, Y. Xu, S. Zhu, F. Cai, J. Liu, Y. Wei and Y. Huang, *ACS Appl. Mater. Interfaces*, 2022, **14**, 33383–33391.
24 W. Shao, H. Wang, F. Ye, C. Wang, C. Wang, H. Cui, K. Dong, Y. Ge, T. Wang, W. Ke and G. Fang, *Energy Environ. Sci.*, 2022, **16**, 252–264.
25 T. Niu, L. Chao, W. Gao, C. Ran, L. Song, Y. Chen, L. Fu and W. Huang, *ACS Energy Lett.*, 2021, **6**, 1453–1479.
26 M. Shahiduzzaman, E. Y. Muslih, A. K. M. Hasan, L. Le Wang, S. Fukaya, M. Nakano, M. Karakawa, K. Takahashi, M. Akhtaruzzaman, J. M. Nunzi and T. Taima, *Chem. Eng. J.*, 2021, **411**, 128461.
27 M. Li, C. Zhao, Z. K. Wang, C. C. Zhang, H. K. H. Lee, A. Pockett, J. Barbé, W. C. Tsoi, Y. G. Yang, M. J. Carnie, X. Y. Gao, W. X. Yang, J. R. Durrant, L. S. Liao and S. M. Jain, *Adv. Energy Mater.*, 2018, **8**, 1801509.
28 C. Gao, H. Dong, X. Bao, Y. Zhang, A. Saparbaev, L. Yu, S. Wen, R. Yang and L. Dong, *J. Mater. Chem. C*, 2018, **6**, 8234–8241.
29 Z. Lin, X. Xu, H. Dong, Q. Song, H. Duan and C. Mu, *ACS Appl. Mater. Interfaces*, 2023, **15**, 1097–1104.
30 W. Pan, J. Lin, J. Wu, B. Rong, X. Zhang, Q. Chen, M. Zhang, S. Wang, W. Sun, X. Wang and Z. Lan, *Sol. Energy*, 2022, **232**, 304–311.
31 F. Wang, D. Duan, K. Zhou, Y. Z. B. Xue, X. Liang, X. Zhou, C. Ge, C. Zhou, J. Xiang, J. Zhu, Q. Zhu, H. Lin, Y. Shi, Y. Chen, G. Li and H. Hu, *InfoMat*, 2023, **5**, e12459.
32 Y. Zhang and N. G. Park, *Adv. Funct. Mater.*, 2023, **33**, 2308577.

33 Y. Cao, J. Feng, Z. Xu, L. Zhang, J. Lou, Y. Liu, X. Ren, D. Yang and S. Liu, *InfoMat*, 2023, **5**, e12423.
34 L. Zheng, L. Shen, Z. Fang, P. Song, W. Tian, J. Chen, K. Liu, Y. Luo, P. Xu, J. Yang, C. Tian, L. Xie and Z. Wei, *Adv. Energy Mater.*, 2023, **13**, 2301066.
35 Y. Ma, C. Zeng, P. Zeng, Y. Hu, F. Li, Z. Zheng, M. Qin, X. Lu and M. Liu, *Adv. Sci.*, 2023, **10**, 2205072.
36 H. Zhu, S. Teale, M. N. Lintangpradipto, S. Mahesh, B. Chen, M. D. McGehee, E. H. Sargent and O. M. Bakr, *Nat. Rev. Mater.*, 2023, **8**, 569–586.